Transition between extended and localized states in a one-dimensional incommensurate optical lattice

Roberto B. Diener, Georgios A. Georgakis, Jianxin Zhong, Mark Raizen, and Qian Niu
Department of Physics, University of Texas, Austin, Texas 78712
(Received 7 March 2001; revised manuscript received 15 May 2001; published 16 August 2001)

We study the localization properties of a one-dimensional incommensurate potential in the full quantum regime. In the system under consideration, and for amplitudes of the potential that are not too weak, the spectrum contains both localized and extended states, with one or more mobility edges. We show how these properties can be experimentally studied through the diffusion of wave packets in a one-dimensional incommensurate optical lattice.

DOI: 10.1103/PhysRevA.64.033416 PACS number(s): 32.80.Lg, 73.20.Fz, 03.65.−w, 02.60.Cb

I. INTRODUCTION

The quantum transport properties of a system are intimately related to the underlying symmetries of the Hamiltonian. In a perfectly periodic system all the eigenfunctions are extended Bloch waves [1], while for a random potential in a quasi-one-dimensional system all the eigenfunctions are localized [2]. These properties can be experimentally studied through the dispersion of an initially localized wave packet; in the former case it grows ballistically, while in the latter the dispersion remains constant.

In between these two extreme cases lie incommensurate and quasiperiodic systems. In these, the spectrum can range from having all extended states to all localized states or even to mixed behavior, as the parameters describing the system (incommensurability, potential amplitude, etc.) are varied. For instance, in the Fibonacci lattice [3] all states are critical (neither localized nor extended), leading to anomalous dispersion. Another known example is the Harper model [4], which models electrons in a two-dimensional lattice in the presence of a transverse magnetic field. The eigenfunctions for this model undergo a transition from localized to extended behavior as the amplitude of the potential of the lattice is decreased. These quantum properties could be related to the quite anomalous transport properties of quasicrystals [5]. These materials show large resistivity and a decreasing temperature dependence; this behavior is enhanced in cleaner samples, thus showing that impurities improve the transport instead of degrading it. A study of transport in a defect-free incommensurate system can then shed some light on the physics underlying quasicrystals.

Such a system can be produced using ultracold atoms in a laser-generated incommensurate optical lattice. Optical lattices have been extensively used to study fundamental quantum-mechanical effects, including Bloch oscillations [6], the existence of Wannier-Stark ladders [7], and nonexponential decay [8]. Two-dimensional quasiperiodic optical lattices have been studied both experimentally and numerically in the incoherent and dissipative regime, in which there is no localization [9]. In one dimension, there have been proposals for using an incommensurate optical lattice as a diffraction grating (with the atoms interacting with the laser fields for a short time) [10] as well as for a study of the dispersion properties in the tight-binding regime [11]. In this last model, the atoms are restricted to the bottom of potential wells and thus the energies allowed belong to a narrow energy interval; the system was shown to be analogous to a generalized Harper model.

We study the motion of atoms in a continuous incommensurate lattice, without any *a priori* restriction on the allowed energies of the particles. Thus, effects in which several energy levels in the wells as well as levels outside of the wells are relevant are automatically included. These energy levels bring into the problem, as we shall show, a richer set of phenomena. For large enough amplitudes of the potential the spectrum contains extended and localized states at high and low energies, respectively. Our study shows that the transition between these two extrema can be nontrivial, with the presence of more than one mobility edges for certain values of the amplitude. We also show how these mobility edges can be experimentally seen using optical lattices.

The paper is organized so as to acquaint the reader with the main ideas used to study incommensurate systems (Secs. I–III), as well as to show the new results obtained and their possible experimental study (in Secs. IV and V). In Sec. II we outline the experimental setup that allows for the construction of an incommensurate optical lattice. The spectrum of the system is studied in Sec. III. In Sec. IV we study the localization properties of the wave functions, and the transition(s) between the localized and extended states in the spectrum. In Sec. V we show how these results can be exhibited experimentally.

II. OPTICAL LATTICES

Optical lattices are produced by the interaction of (neutral) alkali-metal atoms with laser beams operating at a frequency far-detuned from an internal transition. This interaction acts on the external degrees of freedom as a force proportional to the intensity of the laser light [12], while leaving the atoms themselves in the (internal) ground state. A periodic optical lattice is obtained by setting up a standing wave with counterpropagating laser beams (typically, the same beam reflected with optics). The motion of the atoms can be restricted to one dimension by applying high-intensity standing waves in the two perpendicular directions, which localize the atoms to single potential wells in those direc-

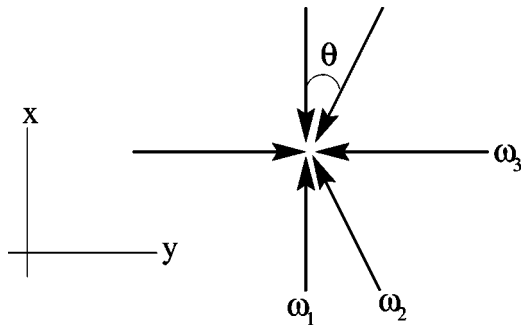

FIG. 1. Diagram of the setup used to obtain a one-dimensional incommensurate optical lattice. An additional pair of counterpropagating laser beams with frequency ω_4 is positioned along the z axis, perpendicular to the diagram. Both these beams and the ones operating at ω_3 have an intensity large enough to restrict the motion of the atoms to the x direction.

tions. All the standing waves work at slightly different detunings to prevent cross-interaction between the atoms and the beams.

An incommensurate potential in one dimension can be obtained as shown in Fig. 1 [10]. The atoms are able to move in the x direction, but are localized in the yz plane. The beams working at ω_1 and ω_2 generate periodic potentials along x with different wave numbers $2K_{L1}$ and $2K_{L2}$. Notice that $2K_{L2}$ can be varied with the angle θ, since $K_{L2}=K_{Laser}\cos\theta$. The Hamiltonian for the atoms is then

$$H=\frac{p^2}{2m}+V_1\cos(2K_{L1}x+\phi)+V_2\cos(2K_{L2}x), \quad (2.1)$$

where m is the mass of the atoms and ϕ is a relative phase between the two standing waves. The amplitudes V_1 and V_2 can be adjusted by varying the intensity of the laser beams. The localization properties of the quantum states of the system are independent of the value of ϕ, but it is important that this phase remains constant throughout an experimental run. This can be achieved by phase locking the laser beams working at ω_1 and ω_2.

We will, in what follows, use a system of units in which $m=\hbar=2K_{L1}=1$. In an experiment with sodium atoms, this corresponds to a unit of time of the order of a microsecond and a unit of energy equal to eight photon recoils. We define $\alpha=K_{L2}/K_{L1}$ and take $\alpha<1$ without loss of generality. The potential energy of the system is then of the form

$$V(x)=V_1\cos(x+\phi)+V_2\cos(\alpha x). \quad (2.2)$$

For simplicity, we will concentrate on the case in which both cosines have the same amplitude, $V_1=V_2=V_0$.

When α is an irrational number, this potential is an incommensurate function of position. In Fig. 2 we show a plot of this function for a particular value of α. Although the potential might look somewhat random, there is a great deal of correlation between the location and height of the wells.

Analytical studies of the spectral properties of continuous incommensurate Hamiltonian systems have shown that for all values of V_0 and at very high energies the spectrum is

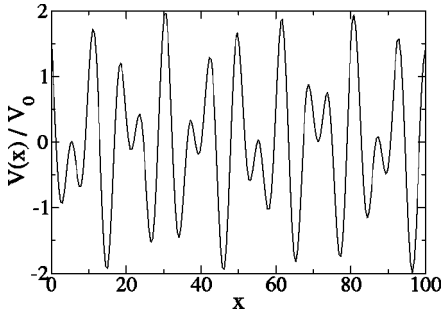

FIG. 2. Potential energy as a function of position, for $\phi=1$ and $\alpha=\gamma$, the inverse of the golden mean.

absolutely continuous, with extended wave functions [13]. It is known that if $V_0\ll 1$ there is no point spectrum (localized states) in the system, while for large enough values of V_0 there are localized states at low energies [14,15]. For these values of V_0 we have a transition between localized and extended states at the two extremes of the spectrum. In physical terms, if the potential wells are deep enough, then the low-lying levels are localized as in a random potential; and for very large energies, the energy eigenstates are weakly perturbed plane waves. As we shall see, this transition can exhibit one or several mobility edges, i.e., band gaps across which the localization properties change character.

III. ENERGY SPECTRA

When α is a rational number ($\alpha=p/q$) the potential (2.2) is periodic in space, with a period of $2\pi q$. Using Bloch's theorem [1], the energy eigenvectors can be found in the form $\Psi_{k,E}(x)=e^{ikx}u_{k,E}(x)$, where u conserves the periodicity of the Hamiltonian $u_{k,E}(x+2\pi q)=u_{k,E}(x)$, so we can write

$$\Psi_{k,E}=e^{ikx}\sum_m c_m e^{imx/q}. \quad (3.1)$$

k is called the quasimomentum, which can be restricted to the first Brillouin zone, in our case the interval $(-1/2q,1/2q]$. We can find the energy eigenfunctions of the Hamiltonian as the solutions of the equation

$$\frac{V_0}{2}(c_{m+q}e^{-i\phi}+c_{m-q}e^{i\phi}+c_{m+p}+c_{m-p})+\left[\frac{(k+m/q)^2}{2}-E(k)\right]c_m=0.$$

The energy spectrum is composed of energy bands; a typical plot of these bands for different rational values of α is shown in Fig. 3; in it, each point corresponds to a single (narrow) band.

The spectrum for a given value of α shows three distinct regions. States buried deep in the potential wells belong to energy bands with very narrow widths. High-energy states (located above the top of the potential barriers) are slightly perturbed free particle states (plane waves). On the other hand, the spectrum in the intermediate region shows a rich

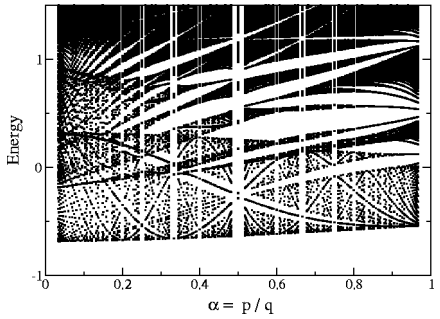

FIG. 3. Energy bands for $V_0=0.5$ and $\phi=0$ as a function of rational $\alpha=p/q$; values with $p<q<30$ are shown. Each point in this plot corresponds to a full (narrow) energy band.

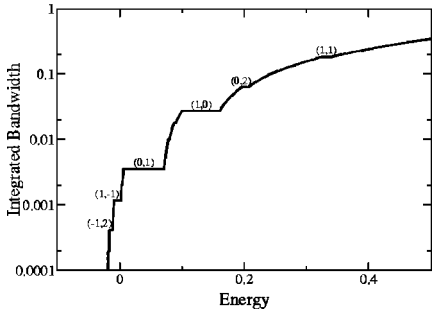

FIG. 4. Integrated bandwidth for $V_0=0.068$, showing the labels for the main gaps in the spectrum.

structure with large energy gaps, reminiscent of the Hofstadter butterfly [16]. This occurs at energies of the order of V_0.

When α is an irrational number Bloch's theorem is no longer applicable and the calculation of the spectrum is nontrivial. This incommensurate case can be studied by taking a sequence of rational numbers $\alpha_n=p_n/q_n$ such that it converges to α as $n\to\infty$. The potential with α_n is called a periodic approximant to the incommensurate potential. One important irrational value for α is the inverse of the golden mean, $\gamma=(\sqrt{5}-1)/2$, which characterizes the quasiperiodicity in some quasicrystals [17] and possesses interesting number-theoretical properties. The sequence of approximants used is obtained by truncating the expansion of γ in terms of a continued fraction, resulting in the recursion $p_n=q_{n-1}, q_n=p_{n-1}+q_{n-1}$ with initial values $p_0=q_0=1$. In the rest of the paper we will study this particular case, although the results are similar for other irrational values of α.

A. Labeling the gaps

As we increase the order n of the approximation, q_n increases and thus the size of the Brillouin zone shrinks, converging to zero. With gaps opening up at both the center and the edges of the Brillouin zone, as $n\to\infty$ gaps open up almost everywhere in the spectrum; the spectrum becomes a Cantor set, which is a fractal [18]. It is of interest to find properties of the system that remain continuous in this limit. As shown by Fig. 3, one such property is the location of the main gaps in the spectrum.

The total number of gaps in the spectrum is infinite, but countable. They can be indexed using the gap-labelling theorem [19]. Given the density of states (per unit length) $\rho(E)$, let us define the integrated density of states $I(E)=\int_{-\infty}^{E}\rho(E)dE$. When evaluated at an energy lying on an energy gap E_{gap} there exists a unique pair of integers n_1 and n_2 such that

$$I(E_{gap})=n_1(1/2\pi)+n_2(1/2\pi\alpha). \tag{3.2}$$

This pair (n_1,n_2) identifies the gap.

It is instructive to plot the integrated bandwidth as a function of the energy. The plots for different rational approximants quickly converge to a curve in the region supporting extended states; the main gaps are displayed as horizontal segments. In Fig. 4 we show the result for $V_0=0.068$, for which the whole spectrum supports extended states. The largest gaps correspond to combinations of small integers n_1 and n_2. If we think of the potential as a perturbation of the free-particle Hamiltonian, then $|n_1|+|n_2|$ is the order of the correction that gives rise to the gap. Thus, integers with larger magnitudes give smaller gaps.

B. Quasimomentum space distributions

For a periodic potential we can calculate the energy as a function of the quasimomentum for the different energy bands. In the quasiperiodic case the quasimomentum is not a well defined quantity, so there is no dispersion relation. In order to study a closely related concept, we plot the eigenfunctions of the Hamiltonian as both a function of momentum p and energy E.

Let us consider first the periodic potential,

$$V(x)=V_0[\cos(x+1)+\cos(x/2)]. \tag{3.3}$$

In the top panel of Fig. 5 we have plotted the energy E as a function of the momentum p for $V_0=0.1$. The gray scale and size of the point represents the probability of measuring a value of p for a given eigenvector of the Hamiltonian with energy E. In the absence of a potential, the plot would just be the free-particle dispersion relation,

$$E=\frac{1}{2}p^2, \tag{3.4}$$

shown as the thick parabola in the lower panel. In the presence of the weak periodic potential (3.3), Bragg scattering with $\Delta p=\pm\frac{1}{2},\pm 1$ becomes possible. Considering multiple-scattering events the momentum can change by integer multiples of $\frac{1}{2}$. We include in the lower panel the free-particle parabola displaced in momentum by such amounts.

We can clearly see in the top panel of Fig 5 the remnants of the free particle parabola, as well as some of the secondary ones. The gaps in the spectrum open up where the energy eigenstates are degenerate, which occurs where two of the parabolas meet. Interpreting the secondary parabolas as Bragg scattered states, the gray scale of the point signals the

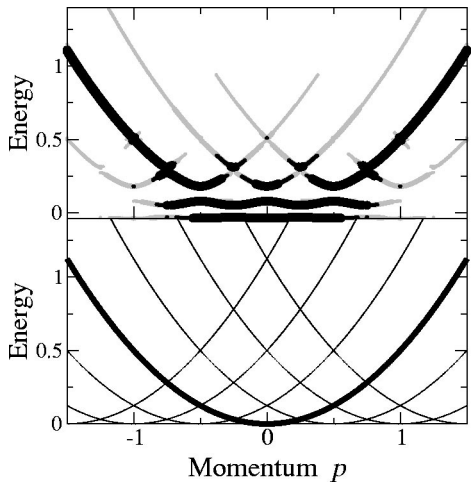

FIG. 5. In the top panel we have plotted the energy versus momentum for the energy eigenstates of a particle moving in the periodic potential (3.3). The points are gray-scale coded, with the gray scale describing the probability of measuring a value of the momentum for an eigenstate of the given energy. In the bottom panel, we have plotted the free-particle parabola (thicker line) together with the same parabola shifted by integer multiples of 1/2.

probability of a particular Bragg scattering, with the gray scale fading as a higher number of scatterings are needed. Notice that if the points were not gray-scale coded in the figure, we would simply obtain the band structure of the system in the repeated-zone scheme [1].

In the case of the quasiperiodic potential

$$V(x)=0.1[\cos(x+1)+\cos(\gamma x)], \tag{3.5}$$

the same plotting method renders Fig. 6. The main difference with the periodic case is in the location of the secondary parabolas; these are not periodically centered in momentum. On the contrary, since we have two incommensurate basis wave vectors, 1 and γ, Bragg scattering occurs with $\Delta p = \pm 1, \pm \gamma$. In general, accounting for multiple scattering, all

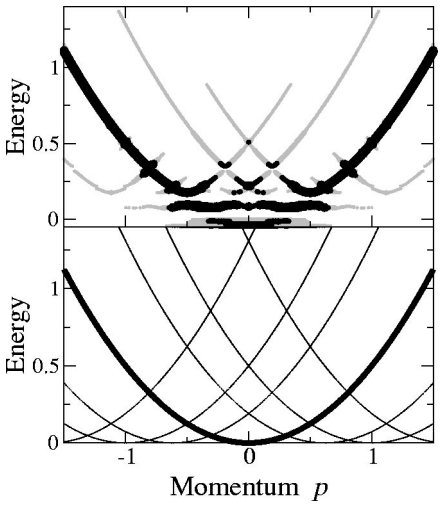

FIG. 6. Same as Fig. 5, but using the potential (3.5).

linear combinations with integer coefficients of 1 and γ are possible. Since these numbers form a dense set on the real line, Δp can take (almost) any value. Thus, without the gray-scale-coding scheme there would be a parabola centered at almost every point and the figure would appear featureless. We can see that the most important parabolas correspond to combinations with small integer values, associated with low-order Bragg scattering. The main gaps open up at the points where these parabolas meet the primary one. The integers used to label the gaps are the same as the ones used to label the center of symmetry of the parabola which gives rise to them.

At low energies the potential completely reshapes the momentum distribution of the energy eigenvectors; as a matter of fact the states deep in the wells become localized in position in the quasiperiodic case. This result is true even at large amplitudes of the potential, with the parabolas being more prominent at energies above the potential barriers.

We can now picture how the energy eigenvectors behave as the potential V_0 is increased adiabatically from zero to a fixed value. Each of the gaps in the spectrum is borne out of the point where the free-particle parabola meets one of the secondary ones. Initially the states are nearly plane waves, but as the potential is increased they become more and more distorted, due to a large number of Bragg scattering events. Every gap can still be uniquely associated with the parabola which in the absence of the potential brings forth a gap at that value of the momentum. Notice that a gap with label (n_1,n_2) opens up at a momentum

$$p_{n_1,n_2}=\frac{n_1+n_2\gamma}{2}. \tag{3.6}$$

IV. LOCALIZATION PROPERTIES

The localization properties of the wave functions of the Hamiltonian can be numerically studied through the scaling properties of the bandwidths. As we increase the value of n, the width of each of the bands decreases. The way in which this decrease scales with the size of the Brillouin zone (q_n) indicates whether the wave functions show extended or localized behavior [20].

For a band with extended states, the bandwidth B_n scales as the inverse of the size of the Brillouin zone q_n^{-1}, or as q_n^{-2} if the band derives from the bottom or the top of a previous approximant (where van Hove singularities arise). On the other hand, localized states belong to bands with the bandwidth decreasing faster than a power of q_n.

Figure 7 shows the scaled bandwidth $B_n q_n$ as a function of the approximation order n (n is proportional to $\ln q_n$) for different situations. In the top panel, we plot the results for the bands between the (1,1) and the (2,0) gaps with an amplitude $V_0=0.5$. These display the behavior typical of bands with extended states; $B_n q_n$ is roughly constant, although some of the bands eventually show a linear decrease in the logarithmic-linear plot, related to the aforementioned van Hove singularities. The middle panel shows the result for a set of bands with localized states [between the (0,2) and the (1,1) gaps for the same amplitude]. These scaled bandwidths

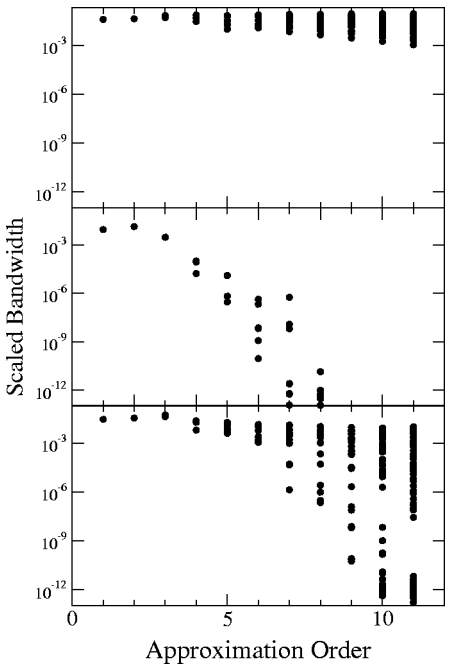

FIG. 7. Scaled bandwidth for a set of extended bands [between the (1,1) and the (2,0) gaps for $V_0=0.5$, top panel], a set of localized bands [between the (0,2) and the (1,1) gaps for $V_0=0.5$, middle panel], and a set undergoing the transition from localized to extended (same bands as in the top panel, with $V_0=0.55$).

decrease rapidly to the numerical error of the calculations, thus there is no scaling with q_n. In the bottom panel we show the scaled bandwidths for the same set of bands used in the top panel but with a larger amplitude, $V_0=0.55$. Some of the bands have undergone a transition to localized behavior, while others still show extended behavior.

From our numerical calculations we see that if a set of labeled bands is localized for a certain value of V_0, then it remains localized for larger values of it. We can then define the value V_0^{tr} for which a set of bands undergoes the extended-localized transition. We have studied the dependence of this value for different bands; the results are plotted in Fig. 8. In order to parametrize the bands we have chosen the momentum $p_{n_1n_2}$ defined by Eq. (3.6). We emphasize

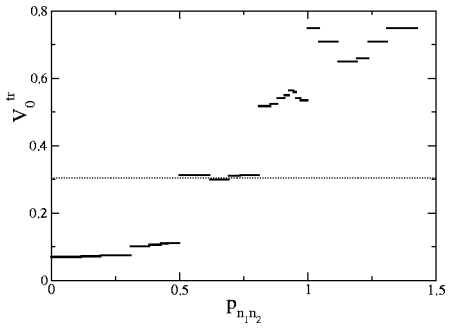

FIG. 8. Amplitude V_0 of the potential at which the extended-localized transition takes place, as a function of the momentum $p_{n_1n_2}$ corresponding to the (n_1,n_2) gap. The horizontal line corresponds to a value of V_0 for which there are three mobility edges.

that the energy of the states is an increasing function of $p_{n_1n_2}$, but this latter parameter is better adapted for devising an experiment.

We want to stress two points from our results. The first one is a calculation of the lowest value of the amplitude for which there are any localized states in the system, $V_0^{min}=0.07$. This can be calculated as the lowest value for which a perturbative expansion of the solution in powers of V_0 diverges. We can also see that there can be more than one mobility edge in the system, since V_0^{tr} is not an increasing function of $p_{n_1n_2}$. For example, when $V_0=0.305$ (marked with a horizontal line in Fig. 8) the states below the (1,0) gap are localized, those between the (1,0) and (0,2) gaps are extended, the ones between the (0,2) and $(2,-1)$ are localized, while higher energy states are ones again extended.

V. WAVE-PACKET DISPERSION

The localization properties can be experimentally studied through the dispersion of wave packets. Numerical studies of wave packet dispersion have been performed in discrete quasiperiodic systems, such as the Fibonacci lattice [21] and the Harper model [22]. In our case, we consider the diffusion of an initially localized wave packet in a quasiperiodic optical lattice. Because of the presence of both types of states in the spectrum for high enough values of V_0, state preparation becomes a crucial step in the design of the experiment.

A. State preparation

The energy resolution of the initial wave packet must be restricted to an interval in which the diffusion properties are approximately uniform; this can be obtained with an adiabatic turn-on of the potential. In general, we want to confine the energy resolution to the interval between two gaps, (n_1,n_2) and (m_1,m_2) (with the former located at a higher energy than the latter). In the absence of the potential, these states correspond to momenta between $p_{n_1n_2}$ and $p_{m_1m_2}$, as argued in Sec. III B. If we prepare a Gaussian wave packet

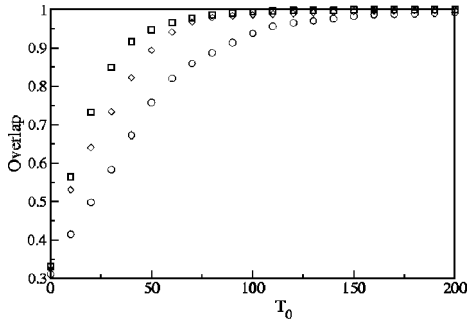

FIG. 9. Overlap probability with the states in the desired energy bands as a function of the turn-on time T_0. The amplitude of the potential in all three cases is $V_0=0.5$ and the initial dispersion in position is $\sigma_x=30$. The circles correspond to an initial momentum $p_0=0.7$ and the desired bands are between the (0,2) and the (1,1) gaps. The squares correspond to $p_0=0.9$ and the bands are between the (1,1) and the (2,0) gaps. Finally, the diamonds correspond to $p_0=1.05$ and the bands are between the (2,0) and the (1,2) gaps.

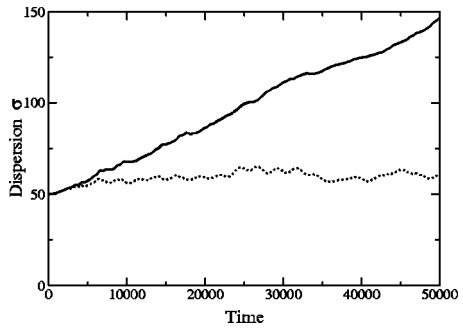

FIG. 10. Dispersion of the wave packets as a function of time for $p_0=0$. The dark curve corresponds to a potential amplitude of $V_0=0.069$, for which there are no localized states. The second curve corresponds to $V_0=0.072$, for which the states around $p_0=0$ are already localized, leading to a localized wave packet. The initial linear increase in both cases is due to the adiabatic turn on of the potential, which occurs during a turn-on time of 2000.

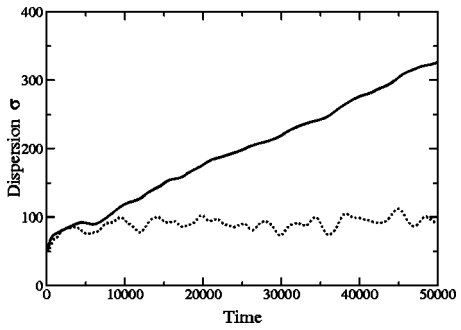

FIG. 11. Dispersion of the wave packets as a function of time for $V_0=0.305$. The full line corresponds to an initial momentum $p_0=0.53$, showing extended behavior. The dotted line corresponds to $p_0=0.65$, for which the underlying states are localized.

with minimum uncertainty, having an initial momentum $p_0=(p_{n_1n_2}+p_{m_1m_2})/2$ and a momentum dispersion $\sigma_p<(p_{n_1n_2}-p_{m_1m_2})/4$ and we turn the potential on slowly enough, then the energy of the wave-packet lies in the desired interval. Notice that the initial dispersion in real space is $\sigma_x=1/(2\sigma_p)$, since the initial wave-packet is a Gaussian with minimum uncertainty. The minimum turn-on time T_0 required to obtain adiabaticity can be estimated as $T_{min}\approx h/\Delta E_g=2\pi/\Delta E_g$, where ΔE_g is the smallest energy gap separating our set of bands to all other bands in the spectrum.

To confirm these results numerically, we assume that the initial wave packet is of the form

$$\Psi(x,t=0)=\frac{1}{\sqrt{2\pi\sigma_x}}\exp\{-(x-x_0)^2/2\sigma_x^2+ip_0x\}, \tag{5.1}$$

where we have taken the initial position of the center of the packet at x_0. We numerically integrate Schrödinger's equation with the amplitude of the potential increasing at a constant rate to its final value V_0 for a time T_0. Using the eigenfunctions of the Hamiltonian, we expand

$$\Psi(x,T_0)=\sum_E a_E(T_0)\psi_E(x). \tag{5.2}$$

The probability that the final state is in the desired set $\mathcal{E}$ of energy states is

$$P(\mathcal{E},T_0)=\sum_{E\in\mathcal{E}}|a_E(T_0)|^2. \tag{5.3}$$

The overlap probability with the states in the desired energy bands as a function of the turn-on time T_0 is shown in Fig. 9 for three different situations. In all three cases, the minimum energy gap $\Delta E_g\approx 0.1$, which implies $T_{min}\approx 60$. This estimate seems to be more accurate for the extended bands than for the localized ones. However, it is seen that the adiabatic turn-on of the potential has the desired effect of rendering a wave-packet localized in energy space.

B. Spreading of the wave packet

For a wave packet prepared in the fashion mentioned, we can numerically integrate the equations of motion to study the quantum diffusion of the wave packet in the lattice. The dispersion is calculated as $\sigma(t)=\sqrt{\langle x^2\rangle-\langle x\rangle^2}$. The evolution of the wave packets exhibits the transition from localized to extended behavior. In Fig. 10 we show the results for a wave packet initially at rest ($p_0=0$) for different values of V_0. For $V_0=0.069$ the wave packet spreads ballistically, with its width increasing linearly with time. On the other hand, at $V_0=0.072$ the wave packet does not spread, thus the energy states making up the wave function are localized. This is confirmed in Fig. 8, which shows that the states around $p_0=0$ undergo the transition at $V_0^{tr}=0.07$.

Another interesting case we show is one in which there are several mobility edges. For $V_0=0.305$ there are localized states at an energy higher than some extended states. The results are shown in Fig. 11. For an initial momentum $p_0=0.53$ [corresponding to energy states between the (1,0) and (0,2) gaps] the wave packet spreads ballistically, while for $p_0=0.65$ [between the (0.2) and $(2,-1)$ gaps] the wave packet remains localized.

Our work shows that the transition between extended and localized states in an incommensurate optical lattice can exhibit more than one mobility edges. These localization properties can be studied experimentally using an atom optical system with parameters that are currently available. A study in a clean, defect-free system will improve the understanding of the intrinsic transport properties of quasicrystals, which are strongly affected by impurities in condensed matter samples.

ACKNOWLEDGMENTS

This work was supported by the NSF and the R. A. Welch Foundation.

[1] Michael Marder, *Condensed Matter Physics* (Wiley, New York, 1999).
[2] P.W. Anderson, Phys. Rev. **109**, 1492 (1958).
[3] M. Kohomoto, L. Kadanoff, and C. Tang, Phys. Rev. Lett. **50**, 1870 (1983).
[4] S. Aubry and G. Andre, Ann. Isr. Phys. Soc. **3**, 133 (1980).
[5] O. Rapp, in *Physical Properties of Quasicrystals*, edited by Z.M. Stadnik (Springer, Berlin, 1999).
[6] M. Ben Dahan, E. Peik, J. Reichel, Y. Castin, and C. Salomon, Phys. Rev. Lett. **76**, 4508 (1996).
[7] S.R. Wilkinson, C.F. Bharucha, K.W. Madison, Qian Niu, and M.G. Raizen, Phys. Rev. Lett. **76**, 4512 (1996).
[8] S.R. Wilkinson, C.F. Bharucha, M.C. Fisher, K.W. Madison, P.R. Morrow, Q. Niu, B. Sundaram, and M.G. Raizen, Nature (London) **387**, 575 (1997).
[9] L. Guidoni, B. Depret, A. di Stefano, and P. Verkerk, Phys. Rev. A **60**, R4233 (1999); L. Guidoni, C. Triché, P. Verkerk, and G. Grynberg, Phys. Rev. Lett. **79**, 3363 (1997).
[10] J.L. Cohen, B. Dubetsky, and P.R. Berman, Phys. Rev. A **60**, 3982 (1999).
[11] K. Drese and M. Holthaus, Phys. Rev. B **55**, R14 693 (1997).
[12] Cohen-Tannoudji, in *Fundamental Systems in Quantum Optics*, edited by J. Dalibard, J.M. Raimond, and J. Zinn-Justin, 1990 Les Houches Lectures (Elsevier, New York, 1992).
[13] E.J. Dinaburg and Ya.G. Sinai, Funct. Anal. Appl. **9**, 279 (1975).
[14] S. Surace, Trans. Am. Math. Soc. **320**, 321 (1990).
[15] J. Fröhlich, T. Spencer, and P. Wittwer, Commun. Math. Phys. **132**, 5 (1990).
[16] Douglas R. Hofstadter, Phys. Rev. B **14**, 2239 (1976).
[17] C. Janot, *Quasicrystals, A Primer* (Oxford Science Publications, Oxford, 1994).
[18] B. Simon, Adv. Appl. Math. **3**, 463 (1982).
[19] J. Bellissard, in *From Number Theory to Physics*, edited by J.M. Luck, P. Moussa, and M. Waldschmidt, Les Houches 1989 (Springer, Berlin, 1993).
[20] H. Hiramoto and M. Kohmoto, Int. J. Mod. Phys. B **6**, 281 (1992).
[21] H. Hiramoto and S. Abe, J. Phys. Soc. Jpn. **57**, 230 (1988).
[22] H. Hiramoto and S. Abe, J. Phys. Soc. Jpn. **57**, 1365 (1988).